Responses to RC2:

The authors need to address the following major points.

Response: We thank the reviewer for insightful and very pertinent comments to improve the paper.

1. The motivation of this manuscript is to address the following issues raised by the authors, the first issue is the Chen et al (2020) method is not applied on a global scale, the second issue is that 'Zhang et al (2016) noted that satellite –measured multi-spectral reflectance of ground-based data alone was not sufficient to retrieve FMFs with high accuracy' (the meaning of this sentence is not quite clear to me), my interpretation is that the use of (only) spectral information from satellite measurements is not enough for the retrieval of FMF, this two reasons are not really solid enough to continue the work proposed in this manuscript. Both manuscripts mentioned above focus on the original level 2 spatial scale (with a very quick look at these two papers), while this work focuses on the level 3 data, the average of spatial resolution from kilometre to degree can make all problems significantly easier, both technically and scientifically. Even later, the authors point to their own previous publication (Yan et al., 2021b) and claimed 'As shown by Yan et al. (2021b), the global land Phy-based FMF is still unreliable.', in which the authors even started 'seasonal FMF characteristics and trends' analysis using the 'unreliable' dataset. This is quite misleading for the understanding of the motivation for the developments in this manuscript, even from the very first step. I think the work should start from level 2 dataset rather than level 3.

Response: Thank you for this question. The key motivation for our paper is to improve the MODIS-based global land FMF retrieval accuracy. The MODIS-based global aerosol product MOD08/MYD08 does not include FMF data because of its high uncertainty. In this study, we only use MODIS level 3 data (i.e., AOD and AE from the MOD08 product) because it is more accurate than level 2 data (Kharol et al., 2011).

We mention the issue "Zhang et al. (2016) noted that satellite-measured multi-spectral reflectance of ground-based data alone was not sufficient to retrieve FMFs with high accuracy" because O'Neill et al. (2008) showed that when the temperature is low, the error of the fine-mode AOD calculated by the physical method, i.e., the Spectral Deconvolution Algorithm (SDA), is clearly large (SDA technical memo, O'Neill et al., 2008, **Figure R1**). So if we want to obtain more accurate FMF retrievals, meteorological variables must be considered. However, the relationship between meteorological factors and FMF is complex, difficult to describe by equations. Therefore, we used a deep-learning model to consider the impact of meteorological factors. This is another motivation of this research. We mention the issue "As shown by Yan et al. (2021b), the global land Phy-based FMF is still unreliable." We note that Yan et al. (2021b) still used the SDA to calculate the FMF without considering the impact of meteorological factors.

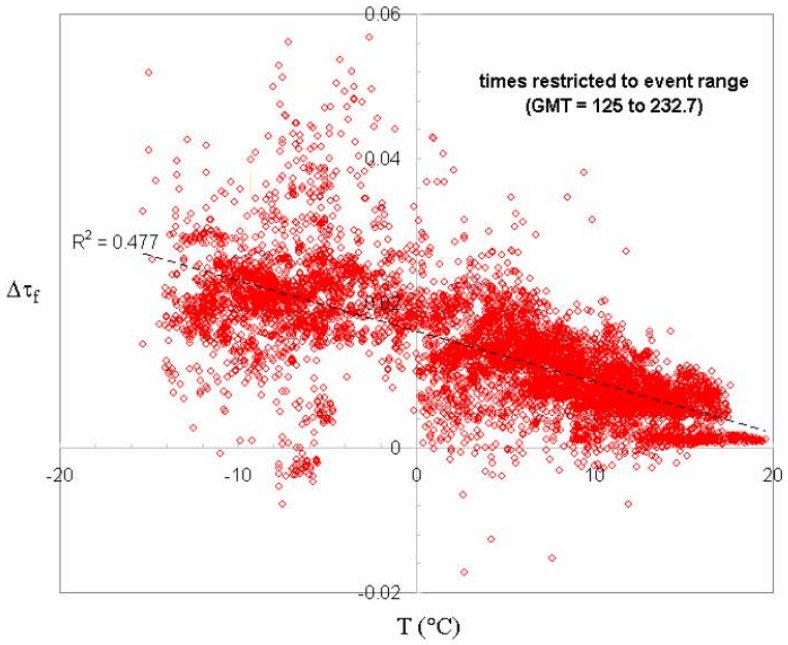

Figure R1. Variation in $\Delta\tau_f$ with detector temperature (PEARL CIMEL, May 1 to August 31, 2007). Copied from the Spectral Deconvolution Algorithm (SDA) Technical memo.

Changes in the manuscript: In the Introduction, we express the motivation more clearly as follows:

Zhang et al. (2016) noted that satellite-measured multi-spectral reflectance of ground-based data alone was not sufficient to retrieve FMFs with high accuracy. O'Neill et al. (2008) showed that when the temperature is low, the error of the fine-mode AOD calculated by the physical method, i.e., the Spectral Deconvolution Algorithm (SDA), is clearly large (SDA technical memo, O'Neill et al., 2008). Although this issue has long been known, the relationship between meteorological factors and FMF is complex, difficult to describe by equations in the SDA. Benefiting from its powerful ability to describe nonlinear relationships, using a deep-learning model may overcome the deficiencies of the SDA in calculating FMFs.

2. The second major point the authors highlighted is that the method is a combination of physical and deep learning approach, this is also quite confusion. As presented in section 2.4, this dataset is created by the new algorithm described in this manuscript for the first time, however, my feeling is that it is a mixture of previous publications without a clear description of the method itself. Meanwhile, the authors mark this paper as a 'Data description paper' in the submission. I never saw a 'Data description paper' without a clear and solid 'Method description paper' before. The key physical part is the LUT-SDA, described in equation (1). Firstly, I am confused why we have two af here? Second, I can not understand how the combination between the physical method and deep learning is achieved. To my personal view, it is still a deep learning method with certain parameters from some physical derivation, however, your major input, aerosol

optical thickness, is derived from a physical model (MODIS retrieval algorithm) as well, you cannot claim it is a combination of physical and deep learning method becuase some inputs for the deep learning is from a product derived from a physical method.

Response: There are three modes for the combined physical and machine-learning model shown in **Figure R2** (Prof. Shen Huanfeng, 2021 China Annual Conference on Theories and Methods of Geographic Information Science).

The first mode is called "Concatenation": The physical model outputs as the machine-learning model inputs or the machine-learning model outputs as the physical model inputs (**Figure R3a**), which is the exact mode employed in our study. Shen et al. (2018) also used this mode to estimate $PM_{2.5}$ by integrating the physical retrieval of AOD and other datasets via the deep-learning model.

The second mode is called "Embedding": This mode uses a machine-learning model as the simulator to replace one part of the physical model, accelerating the overall computational process (**Figure R3b**). For example, Krasnopolsky et al. (1998) used the neural network approach to approximate the atmospheric longwave radiation parameterization for the NCAR Community Atmospheric Model, resulting in faster estimation results.

The third mode is called "Integration": This involves adding physical constraints into the objective function to optimize the result by solving the minimum value of this objective function (**Figure R3c**). T. Li et al. (2021) used a geographically weighted loss function, which served as the spatial constraint for building their AOD–$PM_{2.5}$ relationship.

Therefore, our method using the LUT-SDA FMF as input for the deep-learning model is a way of combining physical and machine-learning models, i.e., concatenation.

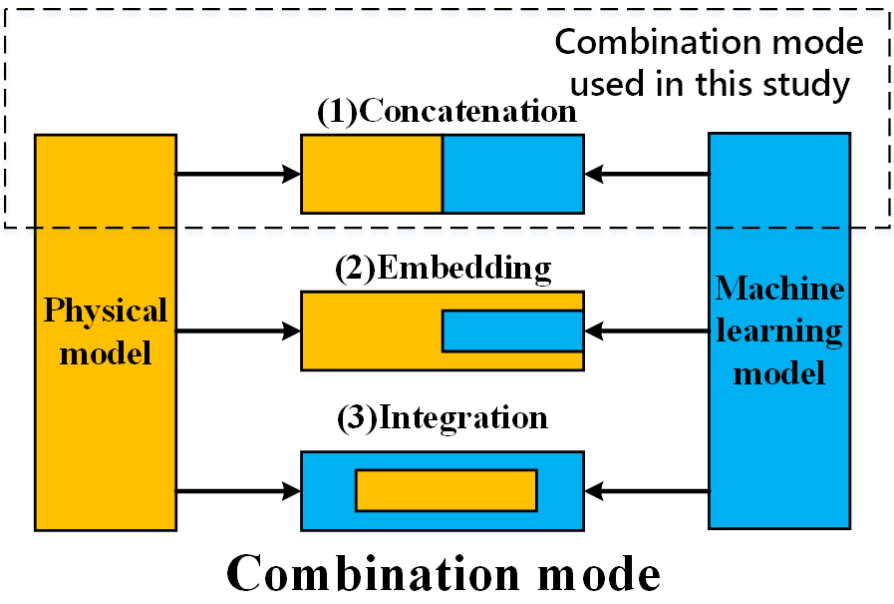

Figure R2. Three combination modes for physical and machine-learning models (copied from the Microsoft PowerPoint presentation prepared by Prof. Shen Huanfeng

and presented at the 2021 China Annual Conference on Theories and Methods of Geographic Information Science).

a. Concatenation:

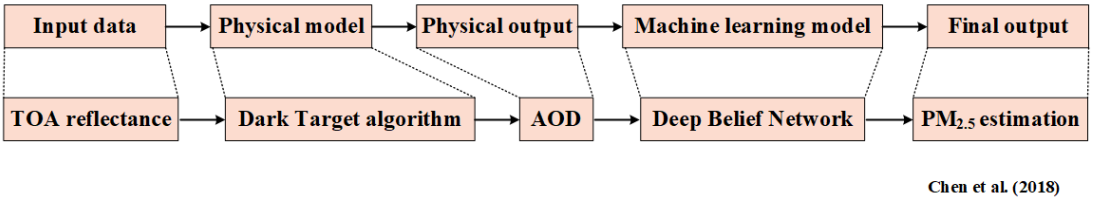

Chen et al. (2018)

b. Embedding:

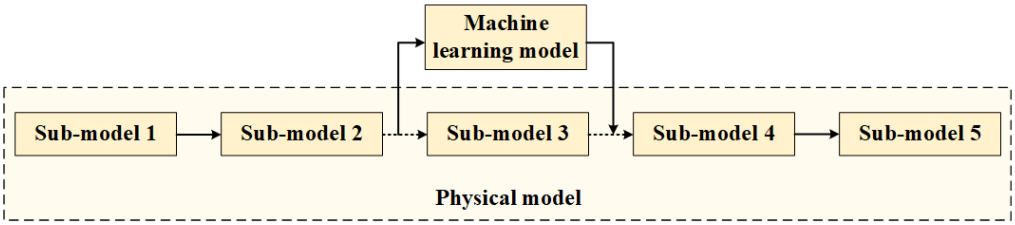

c. Integration:

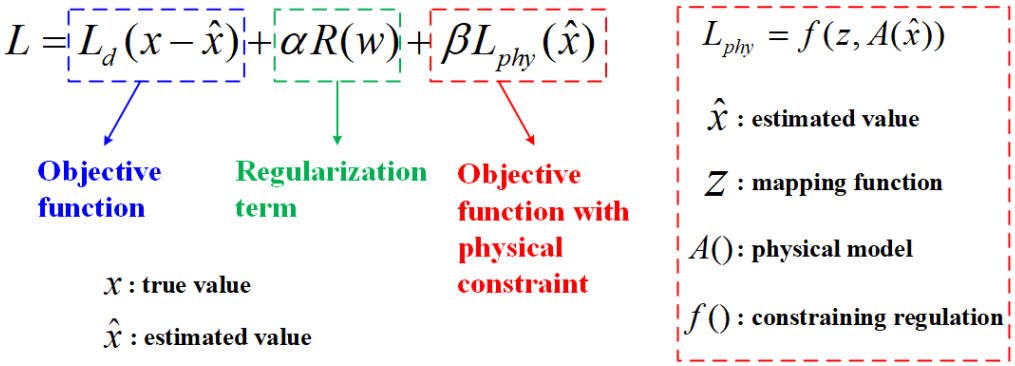

Figure R3. Core structures for the three combination modes (a. concatenation, b. embedding, c. integration) for physical and machine-learning models (copied from the Microsoft PowerPoint presentation prepared by Prof. Shen Huanfeng and presented at the 2021 China Annual Conference on Theories and Methods of Geographic Information Science).

In the revised paper, we have clarified Equation (1). We have also added detailed information about the Phy-DL FMF calculation in the main text and the Supplementary Information document. A new detailed schematic diagram was added to the Supplementary Information document (see Figure S1 below).

Changes in the manuscript:

We added a new figure (Figure 2) to section 2.4 entitled “Combining physical and deep-learning models (Phy-DL) for retrieving FMFs”.

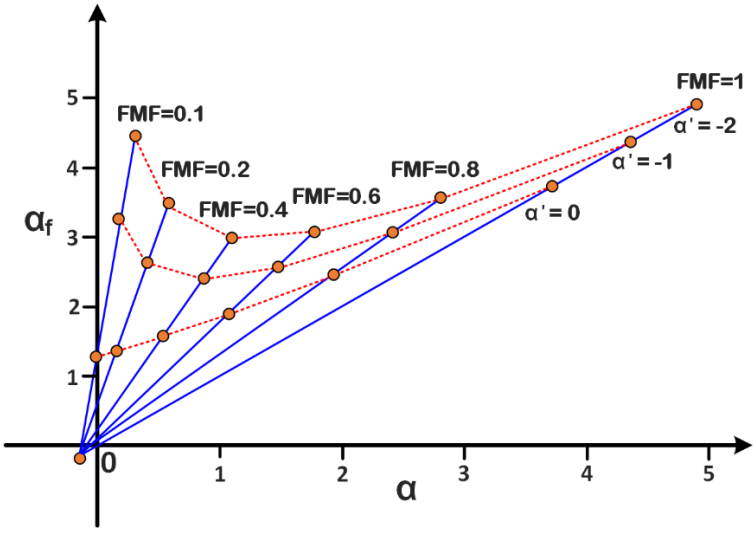

Figure 2. Visual representation of the SDA-based FMF retrieval LUT.

More details in section 2.4:

In this study, we used a "concatenation" mode to combine a physical model and a deep-learning model, i.e., the outputs of the physical model were used as the inputs for the deep-learning model (Figure S1). The physical model used is the LUT-SDA (Yan et al., 2017). The LUT-SDA is designed for satellite FMF retrievals when only AODs at two wavelengths are available (such as DT AOD products). As shown in Eq. (1) of the SDA (O'Neill et al., 2001a), a minimum of AODs at three wavelengths are needed to first obtain the Ångström exponent (AE) derivative (α'). The AE of the fine-mode AOD (α_f) and the FMF can then be calculated.

$$\begin{cases} \alpha_f = \dfrac{1}{2(1-a)} \{(\alpha - \alpha_c - \dfrac{\alpha' - \alpha_c'}{\alpha - \alpha_c} + b^*) + [(\alpha - \alpha_c - \dfrac{\alpha' - \alpha_c'}{\alpha - \alpha_c} + b^*)^2 + 4c^*(1-a)]^{1/2}\} + \alpha_c \\ \mathrm{FMF} = \dfrac{\alpha - \alpha_c}{\alpha_f - \alpha_c} \end{cases} \quad (1)$$

where a, b*, c*, α_c', and α_c are fixed parameters described in section 1 of the Supplementary Information document, based on O'Neill (2010). Since AODs at two wavelengths are not sufficient to calculate α', for the global physically based FMF retrieval, we first divide the whole world into nine regions [as done by Sayer et al. (2014)] and use historical AERONET observed data to determine α' value ranges in these regions. The α' range of values is based on the first and third quartiles of AERONET measurements in different seasons. For example, in Southeast Asia, α' ranges from 0.12 to 0.60 in spring (Yan et al., 2021). In these nine regions, a set of hypothetical values for α' [as determined by Yan et al. (2021)], α_f, and AE (α) are imported into the SDA [Eq. (1)] to build the relationship with FMF (Figure 2).

Different LUTs based on the SDA for these regions are thus created. Based on the constructed LUT, initial results are obtained using a cost function:

$$(FMF^1, \alpha'^1, \alpha_f^{\ 1}) = \min[(LUT - SDA_{AE} - MODIS_{AE})]^2 \quad , \quad (2)$$

where FMF^1, α'^1, and $\alpha_f{}^1$ are uncorrected initial results of FMF, α', and α_f by the LUT-SDA, $LUT-SDA_{AE}$ is the α in the LUT, and $MODIS_{AE}$ is the MODIS MOD08 DT-based AE. After performing the α' bias error correction [described in Supplementary Information, Section 2, O'Neill et al. (2003)] and the mean of extreme (MOE) modification [described in Supplementary Information, Section 3, O'Neill et al. (2008)], the final FMF output is

$$FMF_{\text{output}} = \frac{\alpha - \alpha_c}{\alpha^1_{f\text{corrected}} - \alpha_c} \quad . \qquad (3)$$

We added detailed information about the Phy-DL FMF calculation in the Supplementary Information document:

A new detailed flowchart was added to describe the Phy-DL FMF calculation:

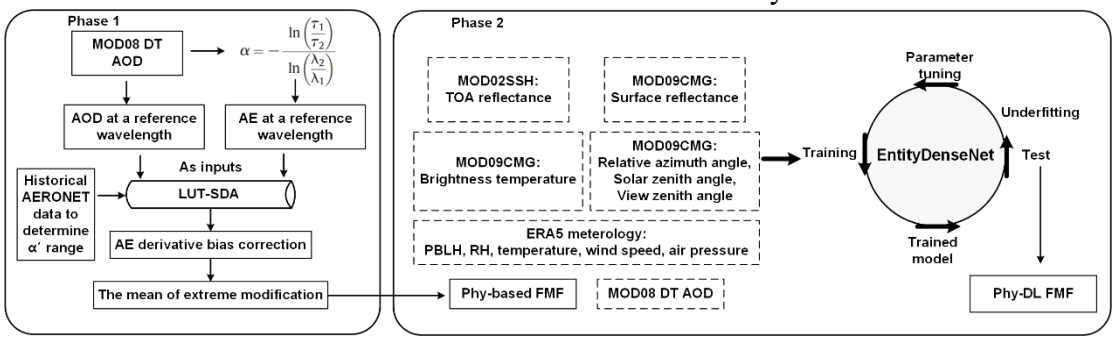

Figure S1. Schematic diagram describing the Phy-DL FMF calculation in this study.

1. The parameters in Eq. (1)

The parameters in Eq. (1) are same as those described by O'Neill et al. (2010):

$$\alpha_f = \frac{1}{2(1-a)}\{(\alpha-\alpha_c-\frac{\alpha'-\alpha_c'}{\alpha-\alpha_c}+b^*)+[(\alpha-\alpha_c-\frac{\alpha'-\alpha_c'}{\alpha-\alpha_c}+b^*)^2+4c^*(1-a)]^{1/2}\}+\alpha_c \quad . \quad (1)$$

The parameters are:

$$\begin{cases} a = (a_{lower} + a_{upper})/2 \\ a_{upper} = -0.22 \\ a_{lower} = -0.3 \end{cases}$$

$$\begin{cases} b^* = b + 2\alpha_c a \\ b = (b_{lower} + b_{upper})/2 \\ b_{upper} = 10^{-0.2388}\lambda^{1.0275} \\ b_{lower} = 0.8 \end{cases}$$

where λ is the reference wavelength (μm). In this study, λ is 0.5 μm.

$$\begin{cases} c^* = c + (b + a\,\alpha_c)\alpha_c - \alpha_c' \\ c = \left(c_{lower} + c_{upper}\right)/2 \\ c_{upper} = 10^{0.2633}\lambda^{-0.4683} \\ c_{lower} = 0.63 \end{cases}$$

$$\alpha_c = -0.15 \text{ and } \alpha_c' = 0$$

2. α' bias error correction

This study used Appendix A1 of O'Neill et al. (2003) to correct the α' bias and propagate this correction through all derived parameters:

$$\alpha'_{error} = 0.65 \times exp[-(FMF^1 - 0.78)^2 / (2 \times 0.18^2)],$$

where FMF^1 is the uncorrected estimate of FMF as shown in Eq. (2) of the main paper. Then

$$\alpha'_{corrected} = \alpha'^1 + \alpha'_{error} \quad ,$$

$$t_{corrected} = \alpha - \alpha_c - \frac{\alpha'_{corrected} - \alpha_c'}{\alpha - \alpha_c} \quad ,$$

$$D_{corrected} = \sqrt{(t_{corrected} + b^*)^2 + 4(1 - a)c^*} \quad ,$$

$$\alpha_{f_{corrected}} = \frac{1}{2(1 - a)}(t_{corrected} + b^* + D_{corrected}) + \alpha_c \quad ,$$

$$FMF_{corrected} = \frac{\alpha - \alpha_c}{\alpha_{f_{corrected}} - \alpha_c} \quad .$$

3. Mean of extreme (MOE) modification

The error in α_f derived by the SDA is (O'Neill et al., 2003):

$$\Delta\alpha_f^2 = \left(k_1\frac{\partial\alpha_f}{\partial\alpha'} + k_2\frac{\partial\alpha_f}{\partial\alpha}\right)^2\left(\frac{\Delta\tau_a}{\tau_a}\right)^2 + \left(\frac{\partial\alpha_f}{\partial a}\Delta a\right)^2 + \left(\frac{\partial\alpha_f}{\partial b}\Delta b\right)^2 + \left(\frac{\partial\alpha_f}{\partial c}\Delta c\right)^2$$

$$+ \left(\frac{\partial\alpha_f}{\partial\alpha'_c}\Delta\alpha'_c\right)^2 + \left(\frac{\partial\alpha_f}{\partial\alpha_c}\Delta\alpha_c\right)^2$$

where $k_1 = 10$, $k_2 = -2.5$, $\Delta\tau_a$ is the nominal root mean square error in AOD at the reference wavelength, τ_a is the AOD at the reference wavelength (in this study, 0.5 μm), $\Delta\alpha'_c = 0.15$, $\Delta\alpha_c = 0.15$, and

$$\begin{cases} \Delta a=(a_{upper} - a_{lower})/2 \\ \Delta b=(b_{upper} - b_{lower})/2 \\ \Delta c=(c_{upper} - c_{lower})/2 . \end{cases}$$

In $\Delta\alpha_f^{\,2}$,

$$\frac{\partial\alpha_f}{\partial\alpha'} = \frac{-1}{FMF_{corrected}\ D_{corrected}},$$

$$\frac{\partial\alpha_f}{\partial\alpha} = \frac{t_+}{FMF_{corrected}\ D_{corrected}} \quad ,$$

$$t_+ = \alpha - \alpha_c - \frac{\alpha'_{corrected} - \alpha_c'}{\alpha - \alpha_c} \quad ,$$

$$\frac{\partial\alpha_f}{\partial a} = \frac{(\alpha_{f_{corrected}} - \alpha_c)}{(1 - a)} + \frac{1}{D_{corrected}} \left(\alpha_c(2\alpha_{f_{corrected}} - \alpha_c) - \frac{c^*}{(1 - a)} \right) \quad ,$$

$$\frac{\partial\alpha_f}{\partial b} = \frac{\alpha_{f_{corrected}}}{D_{corrected}} \quad ,$$

$$\frac{\partial\alpha_f}{\partial c} = \frac{1}{D_{corrected}} \quad ,$$

$$\frac{\partial\alpha_f}{\partial\alpha'_c} = \frac{1}{D_{corrected}} \left(\frac{1}{FMF_{corrected}} - 1\right) \quad ,$$

$$\frac{\partial\alpha_f}{\partial\alpha_c} = \frac{t_{corrected}}{D_{corrected}} \left(\frac{1}{FMF_{corrected}} - 1\right)$$

.

When we obtain the $\Delta\alpha_f$ $(=\sqrt{\Delta\alpha_f^{\,2}})$, the SDA sets the theoretical maximum of α_f as:

$\alpha_{f\,TMAX} = min(4, 10^{(0.18*log10(\lambda)+0.57)})$.

Then,

$\alpha_{f\,MAX} = \alpha_{f_{corrected}} + \Delta\alpha_f$,

$\alpha_{f\,Min} = \alpha_{f_{corrected}} - \Delta\alpha_f$.

If $\alpha_{f\,MAX} > \alpha_{f\,TMAX}$, $\alpha_{f\,MAX} = \alpha_{f\,TMAX}$.

If $\alpha_{f\,Min} > \alpha_{f\,TMAX}$, $\alpha_{f\,Min} = \alpha_{f\,TMAX}$.

The final output of corrected FMF (FMF_{output}) is:

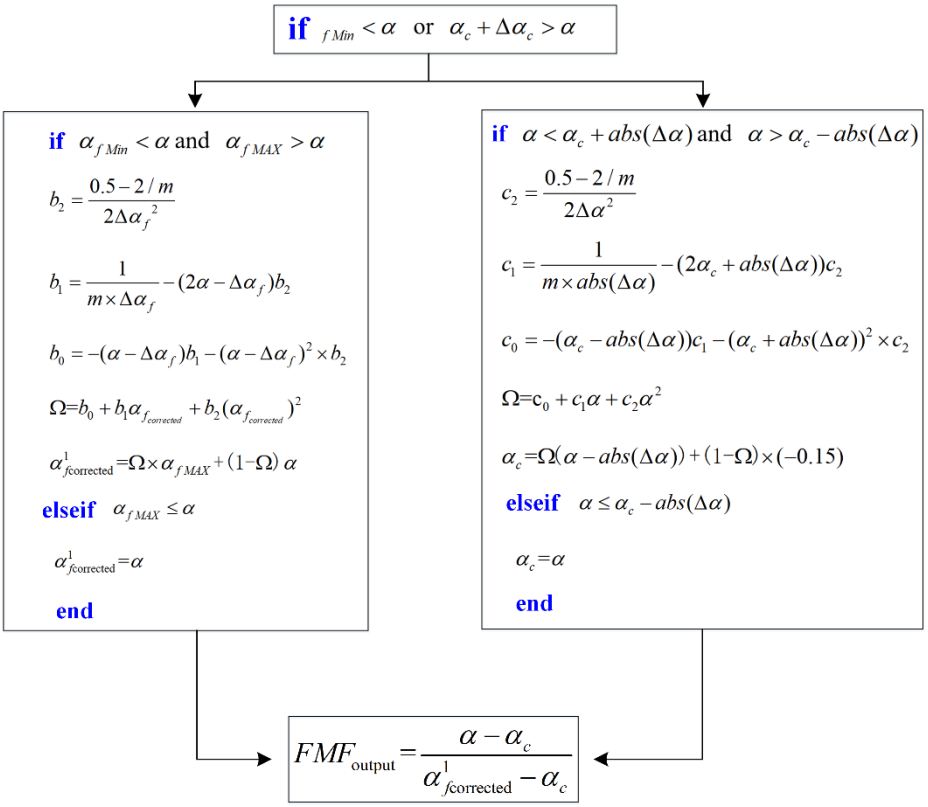

where $m = 8$ and $\Delta\alpha = k_2 \frac{\Delta\tau_a}{\tau_a}$.

3.The third major point is the comparison between different satellite products, the authors need to be aware that it is really the same parameter in the comparison or not, 'bad' agreements between satellite FMF products and the AERONET FMF product do not reveal anything because these FMF are not the same FMF due to different assumptions in particle size distribution and the 'cutting criteria' in the level 2 retrieval process, the FMF derived from this paper is somehow with knowledge (maybe certain inputs as well, not sure about it) from AERONET, it is not surprise at all to have a better agreement with AERONET measurements later. It really makes no sense to include the

MODIS comparison since it is already removed in the new version of dataset. The remove of FMF product in MODIS dataset also indicates how uncertain such a parameter can be.

Response: The validation for satellite FMF products followed Levy et al. (2007) (**Figure R4**). They pointed out that "although the actual products provided by MODIS and AERONET are not necessarily physically identical, in many cases they are comparable", supporting the direct comparison between satellite FMF products and AERONET FMFs. In addition, other validations of satellite FMF products, from POLDER (Wei et al., 2020; Li et al., 2020) to MISR (Dey and Di Girolamo, 2010), also directly used AERONET FMFs for comparison purposes. Zhang et al. (2021) inter-compared their newly retrieved FMFs and MODIS MYD04 FMFs directly with AERONET FMFs (**Figure R5**). Levy et al. (2007) made it clear that "The improvement to the MODIS FMF product is mainly its correlation to AERONET FMF." Therefore, we inter-compared satellite FMF products (from MISR, POLDER, and MODIS) and Phy-DL FMFs directly with AERONET FMFs.

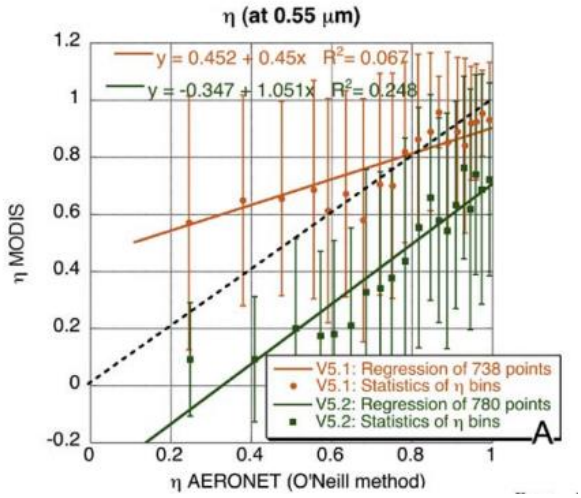

Figure R4. MODIS aerosol size retrievals compared with AERONET derived products. The solid shapes and error bars represent the mean and standard deviation of the MODIS retrievals, in 20 bins of AERONET-derived product. Both the retrievals from V5.1 (orange) and V5.2 (green) are shown. The regressions (solid lines) are for the cloud of all points (not shown). The η over land retrieved at 0.55 mm, compared with AERONET η retrieved by the O'Neill et al. (2003) method. Note that η is defined differently for MODIS and AERONET and that we only show results for $\tau > 0.20$. Copied from Levy et al. (2007).

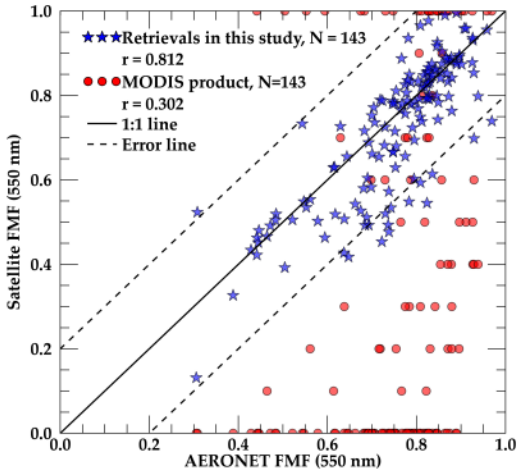

Figure R5. Comparison between the results of this study and MODIS FMFs with AERONET FMFs. Copied from Zhang et al. (2021).

Furthermore, we conducted a validation based on measurements from four independent National Oceanic and Atmospheric Administration Surface Radiation Budget (SURFRAD) network sites not used for training in the deep-learning model. The SURFRAD network provides long-term, multi-bands AOD observations at a temporal resolution of three minutes. As shown in **Figure R6**, the four sites (black triangles) are located across the US, covering different land types from forested land to barren land.

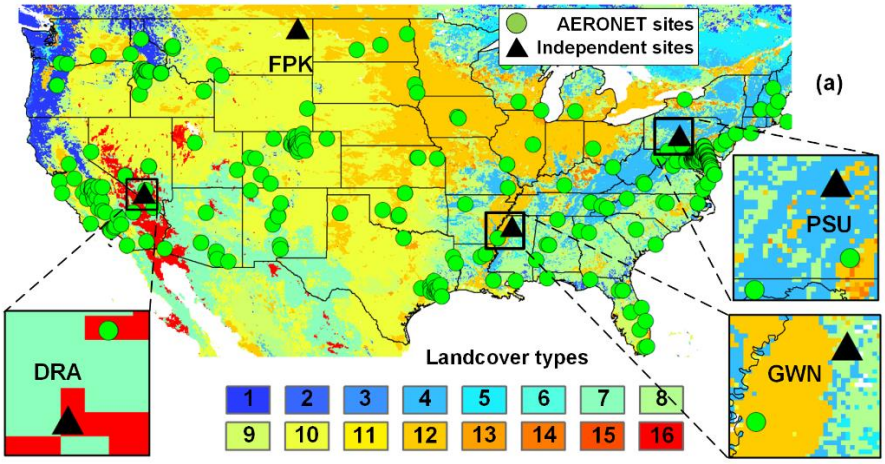

Figure R6. (a) Locations of AERONET sites (green dots) and four independent SURFRAD sites (black triangles, **Table R1**) for the independent validation of the Phy-DL FMF algorithm. The base map shows the land types from MODIS MCD12C1 data (the International Geosphere-Biosphere Programme scheme) in 2010. **Table R2** provides details about the land-type legend.

Table R1. The sites from SURFRAD used for out of site validation and their locations.

Sites	Longitude (°W)	Latitude (°N)	Land type

Desert Rock (DRA)	116.02	36.62	Barren or sparse
Fort Peck (FPK)	105.10	48.31	Grasslands
Goodwin Creek (GWN)	89.87	34.25	Woody savannas
Penn State (PSU)	77.93	40.72	Mixed forests

Table R2. Land types and corresponding values from MODIS MCD12C1 data (the International Geosphere-Biosphere Programme scheme).

Value	Land type	Value	Land type
1	Evergreen needleleaf	9	Savannas
2	Evergreen broadleaf	10	Grasslands
3	Deciduous needleleaf	11	Permanent wetlands
4	Deciduous broadleaf	12	Croplands
5	Mixed forests	13	Urban and built up
6	Closed shrubland	14	Crop natural vegetation mosaic
7	Open shrublands	15	Snow and ice
8	Woody savannas	16	Barren or sparse

The inter-comparison results in **Figure R7** shows that when validated by independent FMF observations not used for training in the deep-learning model (SURFRAD FMFs), Phy-DL FMFs still outperform the other satellite products, with the highest R (0.51), lowest RMSE (0.143), and the greatest number of retrievals falling within the EE envelopes of ±20% (69.08%) and ±40% (89.05%). POLDER and MISR FMFs have the second best performance. PODLER results have an RMSE of 0.232 and R of 0.32, with 76.10% (48.23%) of retrievals falling within the EE envelope of ±40% (20%). MISR results have an R and RMSE of 0.22 and 0.212, respectively, with 82.61% (45.38%) of retrievals falling within the EE envelope of ±40% (20%). MODIS results were the poorest, with an especially high RMSE (0.465) and low percentages of retrievals falling within the EE envelopes of ±40% (37.23%) and 20% (18.09%). Overall, at the independent SURFRAD sites, Phy-DL FMFs are still more accurate and reliable than the other FMF products.

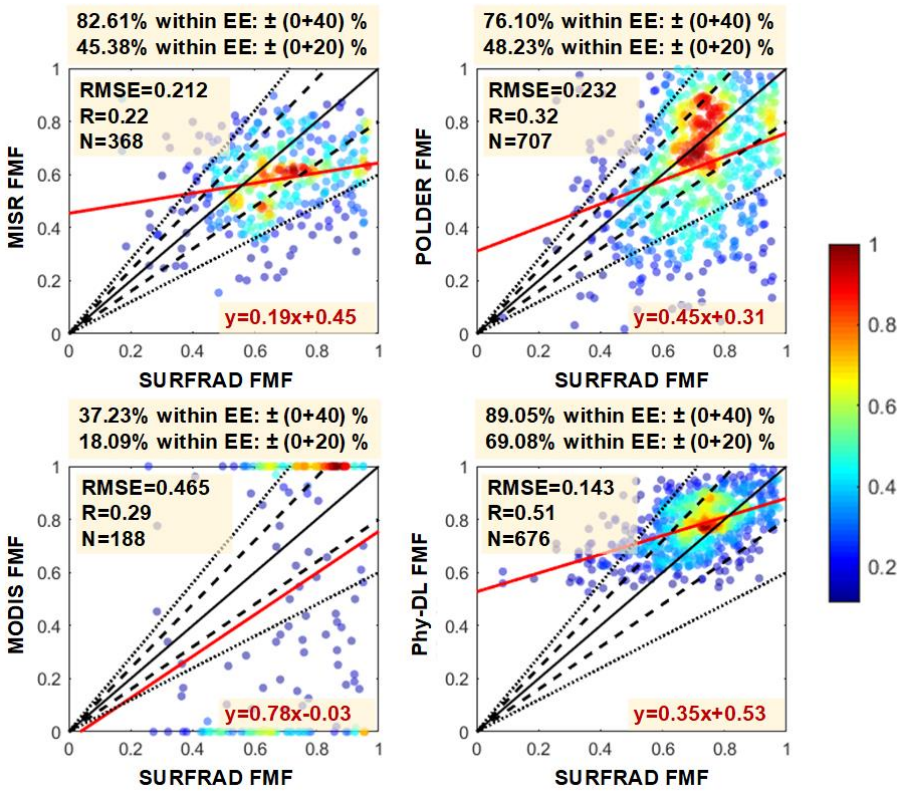

Figure R7. Evaluation of monthly mean (a) MISR (550 nm), (b) POLDER (490 nm), (c) MODIS (550 nm), and (d) Phy-DL FMFs (500 nm) against SURFRAD FMFs (500 nm) from 2008 to 2013. Black and red solid lines are 1:1 reference lines and best-fit lines from linear regression, respectively. Black dashed and dotted lines represent the EE envelopes of ±20% and ±40%, respectively. The number of samples (N), root-mean-square error (RMSE), correlation coefficient (R), and linear regression relation are given in each panel.

Changes in the manuscript:

(1) We have added this validation between independent SURFRAD FMFs and satellite products in the Supplementary Information document:

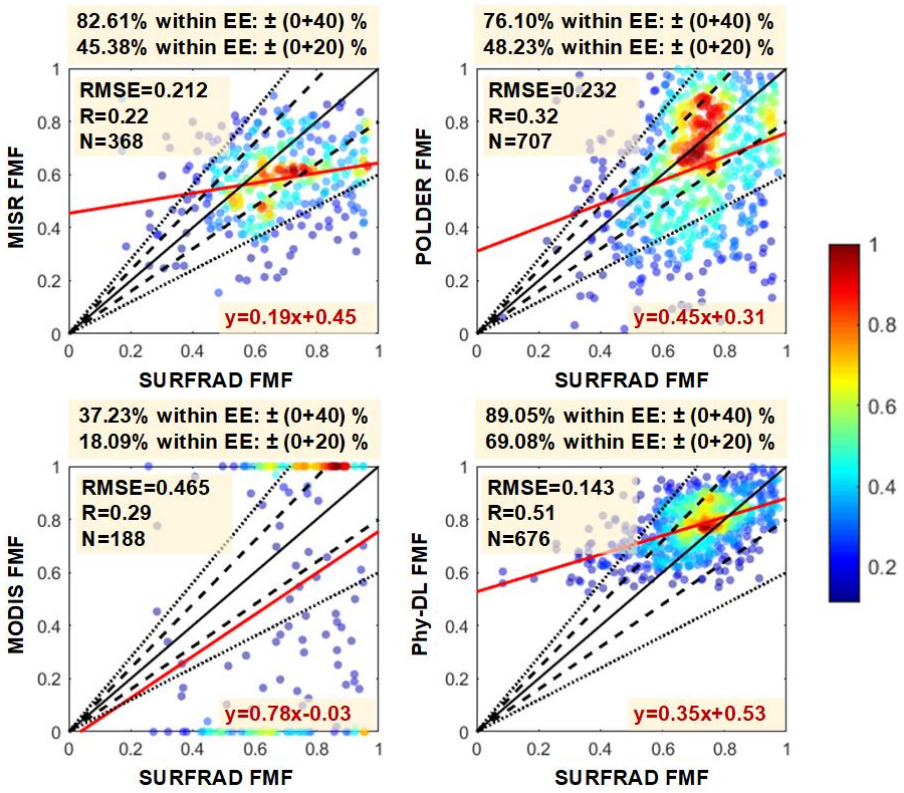

Figure S7. Evaluation of (a) MISR (550 nm), (b) POLDER (490 nm), (c) MODIS (550 nm), and (d) Phy-DL FMFs (500 nm) against SURFRAD FMFs (500 nm) from 2008 to 2013. Black and red solid lines are 1:1 reference lines and best-fit lines from linear regression, respectively. Black dashed and dotted lines represent the EE envelopes of ±20% and ±40%, respectively. The number of samples (N), root-mean-square error (RMSE), correlation coefficient (R), and linear regression relation are given in each panel.

(2) In section 3.4 entitled "Comparison with other satellite-based FMF products", we have added:

The inter-comparison results in **Figure R7** shows that when validated by independent FMF observations not used for training in the deep-learning model (SURFRAD FMFs), Phy-DL FMFs still outperform the other satellite products, with the highest R (0.51), lowest RMSE (0.143), and the greatest number of retrievals falling within the EE envelopes of ±20% (69.08%) and ±40% (89.05%). PODLER results have an RMSE of 0.232 and R of 0.32, with 76.10% (48.23%) of retrievals falling within the EE envelope of ±40% (20%). MISR results have an R and RMSE of 0.22 and 0.212, respectively, with 82.61% (45.38%) of retrievals falling within the EE envelope of ±40% (20%). MODIS results were the poorest, with an especially high RMSE (0.465) and low percentages of retrievals falling within the EE envelopes of ±40% (37.23%) and 20% (18.09%). Overall, at the independent SURFRAD sites, Phy-DL FMFs are still more accurate and reliable than the other FMF products.

4. The fourth major point is the application of this dataset, my personal view is that it

is too early to sell it as a dataset which is mutual enough for a trend analysis, especially since the application of (both fine and coarse as total) aerosol optical thickness is still quite questionable. Even at the last part of the manuscript, the authors claim some significant trends from the new satellite product are not revealed by AERONET measurements due to the scale issue, this simply reveals the limited representative of these AERONET sites in your regions, rather than anything with respect to the satellite data quality.

Response: Thank you for this question. There have been several studies on improving FMF retrievals, some including published datasets, e.g., Chen et al. (2020) (*https://pan.baidu.com/share/init?surl=PhHDLuXv1ltEPZN1wQ68lA,* password: *aero*) and Zhang et al. (2021) (can be requested from the corresponding author: *lizq@radi.ac.cn*). Chen et al. (2020) compared FMF validation studies with a focus on East Asia for different methods (Table R3). Compared with these previous retrieval results, Phy-DL FMF retrievals have better accuracy and lower uncertainty (R=0.68, RMSE=0.136, 90.53% of retrievals falling in the EE envelope of ±40%). Although not highly accurate, many studies have applied these published FMF datasets. Ramachandran (2007) used the MODIS FMF to explore FMF seasonal characteristics in India (**Figure R8**). B. Li et al. (2012) also used the MODIS FMF to investigate the spatial and temporal variations of global fine- and coarse-mode AODs (**Figure R9**). The MODIS global aerosol FMF (MOD08/MYD08) has been recalculated from MODIS regional aerosol products (MOD04/MYD04). Due to the high uncertainty of the MOD04/MYD04 FMF, the latest MODIS C6 global aerosol FMF is no longer available. However, Zhang et al. (2021) used the MODIS C6 MOD04/MYD04 FMF for comparison purposes with their newly retrieved FMF, both plotted as a function of AERONET FMF (**Figure R5**). In addition, Zhang and Li (2015) applied the MODIS C6 MOD04/MYD04 FMF for $PM_{2.5}$ retrievals to isolate the fine-particle contribution (**Figure R10**). Wei et al. (2021) used the FMF derived from POLDER to retrieve PM_{10} over China. The key parameter, the columnar volume-to-extinction ratio VE_{10}, was retrieved by building relationships with FMF (**Figure R11**).

Table R3. Overview of published FMF validation studies with a focus on East Asia for different methods applied to data from multi-spectral sensors. Copied from Chen et al. (2020).

Method	literature	Sensor	RMSE	% in EE[a]	Surface
Collection 6	Levy et al., 2013 validated in Yan et al., 2017 (Table 1)	MODIS	0.340	20%	Dark Target
LUT-SDA	Yan et al., 2017 (Table 1)	MODIS	0.168	80%	Dark Target
NNAero	This paper (Fig. 10d)	MODIS	**0.157**	**91%**	**No Limit**
YAER	Choi et al., 2016 (Fig. 11a)	GOCI	0.264	—[b]	**No Limit**

[a] EE envelopes is ± 0.4.
[b] "—" means not given in the literature.

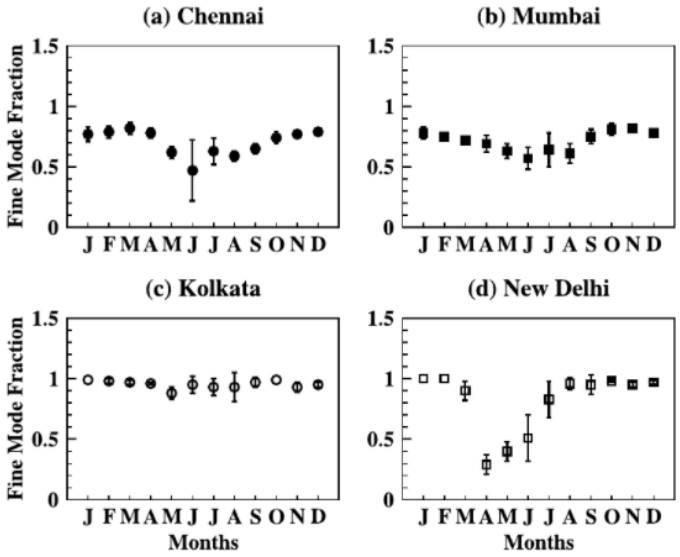

Figure R8. Averaged intra-annual (2001–2005) fine-mode fraction values at (a) Chennai, (b) Mumbai, (c) Kolkata, and (d) New Delhi. Vertical bars denote ±1σ from the mean. Copied from Ramachandran (2007).

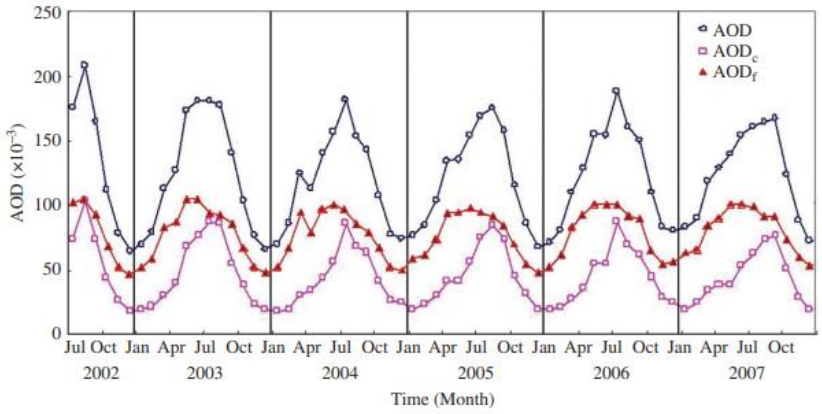

Figure R9. Global inter-annual variation of fine-mode (AOD_f), coarse-mode (AOD_c), and total AOD. Copied from Li et al. (2012).

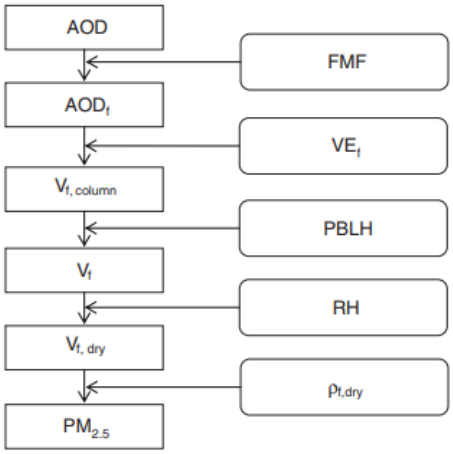

Figure R10. Flowchart of the $PM_{2.5}$ remote sensing method. Copied from Zhang and Li (2015).

$$VE_{10} = 0.3178FMF^2 - 0.8199FMF + 0.69194 \ (0 < FMF \leq 1) \qquad (16)$$

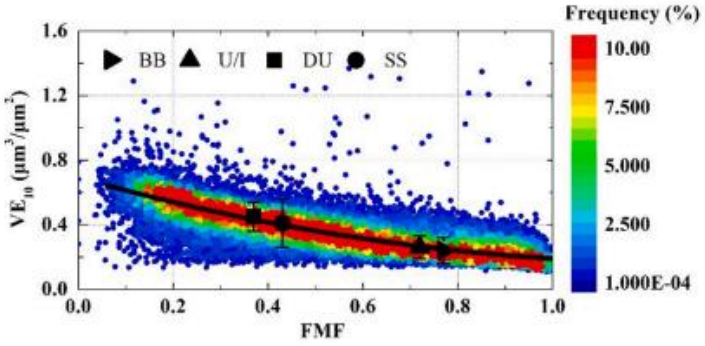

Figure R11. Relationship between the FMF and VE10 at seven typical AERONET sites. Colors represent the frequency of samples in each bin, with FMF intervals of 0.02 and VE_{10} intervals of 0.02 $\mu m^3\ \mu m^{-2}$. There are 1193 valid intervals in total. The black dots and whiskers represent the mean values and standard deviations for four aerosol types. The black solid line shows the fitting curve. Copied from Wei et al. (2021).

This study examined not only the accuracy of Phy-DL FMFs (AERONET validation), but the performances of FMF products from different satellite products using independently derived SURFRAD FMFs (i.e., SURFRAD FMFs not used in the model training). In the revised manuscript, the new SURFRAD validation shows that the Phy-DL FMF retrieval is the most accurate of three FMF products (**Figure R7**). Global trends in Phy-DL and AERONET FMFs over a twenty-year period agreed well. These results suggest that the Phy-DL FMF is reliable enough, even better than existing products. Considering the wide application of MISR and POLDER FMF products that are still highly uncertain, we believe it is reasonable to publish our Phy-DL FMF as a new product, given its demonstrated improved accuracy.

References:

Chen, X., de Leeuw, G., Arola, A., Liu, S., Liu, Y., Li, Z., and Zhang, K.: Joint retrieval of the aerosol fine mode fraction and optical depth using MODIS spectral reflectance over northern and eastern China: artificial neural network method, Remote Sensing of Environment, 249, https://doi.org/10.1016/j.rse.2020.112006, 2020.

Dey, S. and Di Girolamo, L.: A climatology of aerosol optical and microphysical properties over the Indian subcontinent from 9 years (2000–2008) of Multiangle Imaging Spectroradiometer (MISR) data, Journal of Geophysical Research: Atmospheres,115, https://doi.org/10.1029/2009JD013395, 2010.

Kharol, S. K., Badarinath, K. V. S., Sharma, A. R., Kaskaoutis, D. G., and Kambezidis, H. D.: Multiyear analysis of Terra/Aqua MODIS aerosol optical depth and ground observations over tropical urban region of Hyderabad, India, Atmospheric Environment, 45, 1532–1542, https://doi.org/10.1016/j.atmosenv.2010.12.047, 2011.

Krasnopolsky, V. M., Fox-Rabinovitz, M. S., and Chalikov, D. V.: New approach to calculation of atmospheric model physics: accurate and fast neural network emulation of longwave radiation in a climate model, Monthly Weather Review, 133, 1370–1383, https://doi.org/10.1175/mwr2923.1, 2005.

Levy, R. C., Remer, L. A., Mattoo, S., Vermote, E. F., and Kaufman, Y. J.: Second-generation operational algorithm: retrieval of aerosol properties over land from inversion of Moderate Resolution Imaging Spectroradiometer spectral reflectance, Journal of Geophysical Research: Atmospheres, 112, https://doi.org/10.1029/2006jd007811, 2007.

Li, B., Su, S., Yuan, H., and Tao, S.: Spatial and temporal variations of AOD over land at the global scale, International Journal of Remote Sensing, 33, 2097–2111, https://doi.org/10.1080/01431161.2011.605088, 2012.

Li, L., Che, H., Derimian, Y., Dubovik, O., Luan, Q., Li, Q., et al.: Climatology of Fine and Coarse Mode Aerosol Optical Thickness Over East and South Asia Derived From POLDER/PARASOL Satellite. Journal of Geophysical Research: Atmospheres, 125, e2020JD032665, https://doi.org/10.1029/2020JD032665, 2020.Li, T., Shen, H., Yuan, Q., and Zhang, L.: A locally weighted neural network constrained by global training for remote sensing estimation of $PM_{2.5}$, IEEE Transactions on Geoscience and Remote Sensing, 1–13, https://doi.org/10.1109/TGRS.2021.3074569, 2021.

O'Neill, N. T.: Comment on "Classification of aerosol properties derived from AERONET direct sun data" by Gobbi et al. (2007), Atmospheric Chemistry and Physics, 10, 10,017–10,019, https://doi.org/10.5194/acp-10-10017-2010, 2010.

O'Neill, N. T., Dubovik, O., and Eck, T. F.: Modified Ångström exponent for the characterization of submicrometer aerosols, Applied Optics, 40, 2368–2375, https://doi.org/10.1364/ao.40.002368, 2001a.

O'Neill, N. T., Eck, T. F., Smirnov, A., Holben, B. N., and Thulasiraman, S.: Spectral discrimination of coarse and fine mode optical depth, Journal of Geophysical Research: Atmospheres, 108, https://doi.org/10.1029/2002jd002975, 2003.

O'Neill, N., Eck, T., Smirnov, A., and Holben, B. Spectral deconvolution algorithm (SDA) technical memo, 2008.

O'Neill, N. T.: Comment on "Classification of aerosol properties derived from AERONET direct sun data" by Gobbi et al. (2007), Atmospheric Chemistry and Physics, 10, 10017-10019, 10.5194/acp-10-10017-2010, 2010. Ramachandran, S.: Aerosol optical depth and fine mode fraction variations deduced from Moderate Resolution Imaging Spectroradiometer (MODIS) over four urban areas in India, Journal of Geophysical Research: Atmospheres, 112, https://doi.org/10.1029/2007jd008500, 2007.

Sayer, A. M., Munchak, L. A., Hsu, N. C., Levy, R. C., Bettenhausen, C., and Jeong, M. J.: MODIS Collection 6 aerosol products: Comparison between Aqua's e-Deep Blue, Dark Target, and "merged" data sets, and usage recommendations, Journal of Geophysical Research: Atmospheres, 119, 13,965–913,989, https://doi.org/10.1002/2014JD022453, 2014.

Shen, H., Li, T., Yuan, Q., and Zhang, L.: Estimating regional ground-level $PM_{2.5}$ directly from satellite top-of-atmosphere reflectance using deep belief networks, Journal of Geophysical Research: Atmospheres, 123, 13,875–813,886, https://doi.org/10.1029/2018JD028759, 2018.

Wei, Y., Li, Z., Zhang, Y., Chen, C., Dubovik, O., Zhang, Y., Xu, H., Li, K., Chen, J., Wang, H., Ge, B., and Fan, C.: Validation of POLDER GRASP aerosol optical retrieval over China using SONET observations, Journal of Quantitative Spectroscopy and Radiative Transfer, 246, https://doi.org/10.1016/j.jqsrt.2020.106931, 2020.

Wei, Y., Li, Z., Zhang, Y., Chen, C., Xie, Y., Lv, Y., and Dubovik, O.: Derivation of PM_{10} mass concentration from advanced satellite retrieval products based on a semi-empirical physical approach, Remote Sensing of Environment, 256, 112319, https://doi.org/10.1016/j.rse.2021.112319, 2021.

Yan, X., Li, Z., Shi, W., Luo, N., Wu, T., and Zhao, W.: An improved algorithm for retrieving the fine-mode fraction of aerosol optical thickness. Part 1: Algorithm development, Remote Sensing of Environment, 192, 87–97, https://doi.org/10.1016/j.rse.2017.02.005, 2017.

Yan, X., Zang, Z., Liang, C., Luo, N., Ren, R., Cribb, M., and Li, Z.: New global aerosol fine-mode fraction data over land derived from MODIS satellite retrievals, Environmental Pollution, 276, https://doi.org/10.1016/j.envpol.2021.116707, 2021b.

Zhang, Y. and Li, Z.: Remote sensing of atmospheric fine particulate matter ($PM_{2.5}$) mass concentration near the ground from satellite observation, Remote Sensing of Environment, 160, 252–262, https://doi.org/10.1016/j.rse.2015.02.005, 2015.

Zhang, Y., Li, Z., Qie, L., Zhang, Y., Liu, Z., Chen, X., Hou, W., Li, K., Li, D., and Xu, H.: Retrieval of aerosol fine-ode fraction from intensity and polarization measurements by PARASOL over East Asia, Remote Sensing, 8, https://doi.org/10.3390/rs8050417, 2016.

Zhang, Y., Li, Z., Liu, Z., Wang, Y., Qie, L., Xie, Y., Hou, W., and Leng, L.: Retrieval of aerosol fine-mode fraction over China from satellite multiangle polarized

observations: validation and comparison, Atmos. Meas. Tech., 14, 1655-1672, https://doi.org/10.5194/amt-14-1655-2021, 2021.